9

On Adjustable Stiffness Artificial Tendons in Bipedal Walking Energetics

Reza Ghorbani and Qiong Wu
University of Hawaii at Manoa, University of Manitoba
USA, Canada

1. Introduction

Inspired by locomotion in nature, researchers have developed the passive dynamic walking machine principle and applied it to the legged robotics (Coleman & Ruina, 1998; Collins et al., 2001; Garcia, 1999; McGeer, 1990; Wisse, 2004; Wisse & Frankenhuyzen, 2006). The passive dynamic walking machines provide human-like locomotion in legged robots that is more efficient than the precisely joint-angle-controlled robots. On the other hand, tuning the parameters of the passive dynamic walking robots are tricky, time consuming and requires much experimentation. In addition, passive dynamic walking robots still have considerable energy loss through rapid changes in the velocity direction of the center of mass of the robot during collision of the foot with the ground. Precisely joint-angle-controlled bipedal walking robots also undergo significant energy loss caused by rigid collision of the foot with the ground in addition to their common energy dissipation in robot's power systems.
Collision of the foot with the ground during bipedal walking is inevitable which is one of the major sources of the energy loss. Establishing a new technique to reduce this energy loss is a challenging problem which we desire to address in this work by developing the idea of using the adjustable stiffness elastic elements in robot's structure. We believe that the adjustment of the elasticity as a control strategy can significantly improve the energetics of locomotion in bipedal walking robots by reducing the energy loss during the collision phase, which starts with an impact of the heel-strike followed by continuous motion and ends by a second impact at the foot-touch-down. This work , as a first step in this research area, constructively demonstrates the idea through two main efforts. The first effort is to develop the conceptual designs of the adjustable stiffness artificial tendons (ASAT) to show that the idea can be implemented in practice. The second effort is to study the effects of adjustable stiffness elasticity on reducing the energy loss by adding the model of each ASAT into the robot dynamics.
This introductory section reviews the research on legged locomotion which indicates the importance of elasticity in mechanics of locomotion in nature. In human walking, part of the kinetic and potential energy from the body is transiently stored as elastic strain energy during the collision phase and is released later during the rebound phase by elastic recoil (Kuo et al., 2005). This phenomenon greatly reduces the work required from the muscles and lowers the metabolic cost of locomotion (Alexander & Bennett, 1989; Cavagna et al., 1977). The mechanics of elastic recoil were also studied for running and it was found that, the forward kinetic energy of the body's center of mass is in phase with fluctuations in gravitational potential energy (Cavagna et al., 1964). It was also found that, humans and animals most likely store

the elastic strain energy in muscles, tendons, ligaments and perhaps even bones, thereby, reducing the fluctuations in total mechanical energy (Cavagna et al., 1964). It has been reported that the leg stiffness influences many kinematic variables such as the stride frequency and the ground contact time (Farley & Gonzalez, 1996; McMahon & Cheng, 1990). Thus, the stiffness of the leg is a key parameter in determining the dynamics of locomotion (Ferris et al., 1998). He and Farley (Farley et al., 1993; He et al., 1991) suggested that the inherent properties of the musculoskeletal system determine an animal's choice of leg stiffness. Their idea was supported by (Roberts et al., 1997) who exposed that the muscles of running turkeys undergo very little change in length during the ground contact. Thus, the tendon may contribute most of the compliance of the muscle-tendon unit and greatly influence the leg stiffness (Alexander, 1988). In addition, adjusting the elasticity of the muscle-tendon unit during human locomotion contributes significantly to its efficiency. Thus, adjusting the stiffness of the robot's structure can be crucial for its energy economy which is studies in this work .

In the context of developing the legged robots, implementation of the adjustable leg stiffness in a running robot has been recommended by researchers to improve the performance on varied terrain (Ferris et al., 1998). Besides allowing the robot to accommodate different surface conditions, the adjustable leg stiffness would permit a robot to quickly adjust its stride length to avoid obstacles on rocky and uneven surfaces. Research is also plentiful in the area of series elasticity. Many of the ideas, problems and solutions of series elasticity related to this work , are initiated and discussed in publications of the MIT leg lab (Howard, 1990; Pratt & Williamson, 1995; Robinson et al., 1999; Williamson, 1995). Beyond the basics, much of the current research in series elasticity addresses topics such as human centered robotics (Zinn et al., 2004) and running robots (Hurst et al., 2004; Hurst & Rizzi, 2004).

Seyfarth developed a simple model of legged locomotion based on compliant limb behavior which is more similar to the human walking behavior (natural walking) than a traditional model of two coupled pendula (Seyfarth, 2000). Geyer also studied the basics of the compliant walking locomotion (Geyer et al., 2002; 2005). Jena walker II was successfully developed at the University of Jena by continuing the research on efficient locomotion using elasticity. However, the stiffness of elastic element in Jena walker II is constant. The electro–mechanical Variable Stiffness Actuation (VSA) motor developed of the University of Pisa is designed for safe and fast physical human/robot interaction in manipulators (Bicchi & Tonietti, 2004). A series elastic actuation system based on the Bowden–cable was developed at the University of Twente, (Veneman et al., 2006) for manipulator robots applications. The idea of controlling the compliance of a pneumatic artificial muscle to reduce the energy consumption of the robot is practically demonstrated, (Vanderborght et al., 2006). Most of the recent research on compliant locomotion is reported by researchers (Geyer, 2005; Ghorbani, 2008; Ghorbani & Wu, 2009a;b).

However, none of the previous research adequately addresses the specific issues of effects of the adjustable stiffness elasticity on reducing the energy loss in bipedal walking robots through a mechanical design approach. This work seeks to fill that gap through the following stages of designing the adjustable stiffness artificial tendons, studying their effects on energetics of bipedal walking robots and investigating the control issues.

The organization of this work is as follows. Section 2 describe three different conceptual designs of ASAT. The OLASAT is selected to continue of studying the energetics. However more information related to the advantages and limitations of each ASAT, the potential applications of ASAT as well as the effects of ASAT on series elastic actuation systems are explained in articles by authors (Ghorbani, 2008; Ghorbani & Wu, 2009a). In order to capture the ba-

sic behavior of OLASAT, a simple 2–DOF model of bipedal walking is illustrated in section 3. It also summarized the normalized formulation of the equations of motion of the biped. Section 4 contains the calculation of the energy loss at the foot-touch-down. A controller to automatically adjust the stiffness of OLASAT is proposed in section 5. Then in section 6, computer simulations are carried out to demonstrate the effects of stiffness adjustment of OLASAT on energy efficiency during the single support stance phase. The mathematical model of the bipedal walking is developed in sections 3.1 and 3.2.

2. Conceptual Design and Modeling of ASATs

In this section, three different conceptual designs of ASAT are developed. The conceptual designs have not been fabricated in this project. The first design (section 2.1) is a rotary adjustable stiffness artificial tendon that is a bi-directional tendon able to apply torque in a clockwise as well as a counter clockwise direction. The second design (section 2.2) is a unidirectional linear adjustable stiffness artificial tendon that uses the concept of changing the number of active coils of two series springs. Finally, the third design (section 2.3) is a combination of two offset parallel springs that is an unidirectional tendon. The mathematical model of each tendon is developed. The advantages, limitations of each concept and the potential applications to the development of a compliant actuation system are discussed in (Ghorbani & Wu, 2009a).

2.1 Rotary Adjustable Stiffness Artificial Tendon (RASAT)

The Rotary Adjustable Stiffness Artificial Tendon (RASAT) is specially designed to provide a wide range of the angular stiffness. The schematic of RASAT is illustrated in Fig. 1. In RASAT, a pair of compression springs is intentionally inserted between the two concentric input and output links. Each spring pair consists of a low stiffness spring with a stiffness of K_1 and a high stiffness spring with a stiffness of K_2. The offset between the low and high stiffness springs has a constant value of l. Distance d, of the spring pairs with respect to the center of rotation of the links, is adjustable. In this case, the internal torque T, between the concentric input and output links is calculated from:

$$T = \begin{cases} K_1 d\ x = K_1 d^2 \tan\theta & \frac{l}{d} \geq \tan\theta \\ K_1 dl + d(K_1 + K_2)(d\tan\theta - l) & \frac{l}{d} < \tan\theta \end{cases} \quad (1)$$

where θ is the angular displacement between the input and output links, x is the spring deflection. In Equation 1, $\frac{l}{d} > \tan\theta$ represents the situation that only spring 1 is engaged and $\frac{l}{d} < \tan\theta$ is when both springs are engaged. The stiffness of spring 2 is μ times higher than the stiffness of spring 1. Thus:

$$K_2 = \mu K_1 \quad (2)$$

Combining Equations 1 and 2 and converting to the following non-dimensional form:

$$\frac{T}{K_1 d_{max}^2} = \begin{cases} tan\theta(\frac{d}{d_{max}})^2 & \frac{l}{d} > \tan\theta \\ (\mu+1)\tan\theta(\frac{d}{d_{max}})^2 - \mu\frac{l}{d_{max}}(\frac{d}{d_{max}}) & \frac{l}{d} < \tan\theta \end{cases} \quad (3)$$

where d_{max} is the maximum value of distance d. The effects of the distance ratio, $\frac{d}{d_{max}}$, on the output torque index, $\frac{T}{K_1 d_{max}}$, in RASAT are graphically illustrated in Figs. 2 and 3 where $\mu = 5$ and $\frac{l}{d_{max}} = 0.1$. As shown in Fig. 2, by increasing the distance, d, from zero to d_{max}, for a given θ, the torque index, $\frac{T}{K_1 d_{max}}$, increases. This relationship is shown for different θ

while increases from $\theta = 5^o$ to $\theta = 15^o$ with equal steps of 1^o. The torque–angular deflection relation in RASAT is graphically illustrated in Fig. 3 for different values of distance indexes $\frac{d}{d_{max}}$. The slope of each curve in Fig. 3 is equivalent to the stiffness of the tendon. As shown in Fig. 3, by decreasing the ratio $\frac{d}{d_{max}}$, from 1 to 0.1 with steps of 0.1, the slopes of curves are reduced significantly. It has been shown in Fig. 3 that the slopes of the curves can be adjusted in a wide range which illustrates the capability of RASAT in adjusting the stiffness in a wide range. Sudden changes in the slopes of the curves in Fig. 3 are caused by engaging the high stiffness spring. Also, the higher the ratio $\frac{d}{d_{max}}$, the sooner the sudden change occurs. The effect of the stiffness ratio of the springs, μ, on the stiffness of RASAT is illustrated in Fig. 4 by assuming $\frac{d}{d_{max}} = 0.8$ and $\frac{l}{d_{max}} = 0.1$. Increasing the μ represents the increasing of the stiffness ratio of spring 2 to spring 1. In Fig. 4, the slope of the curves increases at the turning point that is caused by engaging spring 2 while μ increases from zero to 5 with equal increment of 1.

From the mechanical design point of view, RASAT (Fig. 5a & 5b) is comprised of an input

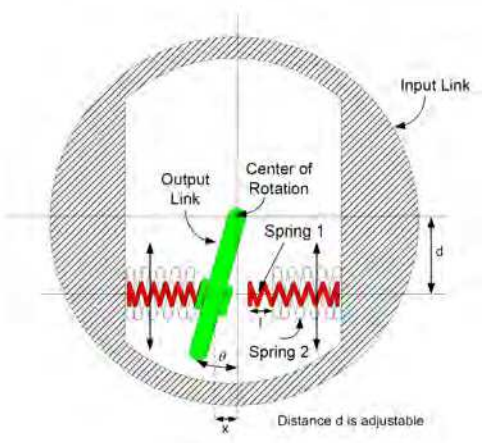

Fig. 1. General schematic of RASAT. A pair of two compression springs (spring 1 and spring 2) with a constant offset, l, are located in each side of the output link. Input and output links are concentric and d, the distance of springs to the center of rotation, is adjustable.

link (Fig. 5d), an output link (Fig. 5c), four springs (not shown in Fig. 5 but is shown in Fig. 1), and the spring positioning mechanism that is installed on the input link as shown in Fig. 5d. Input and output links are concentric and a relative angular displacement between the input and output links, θ, can be measured using a potentiometer installed on the input link (Fig. 5b). Two pairs of parallel helical compression springs configured in an offset are located inside the spring housing. The spring housing is linearly positioned by a non–back drive-able ball screw and a nut, which in turn, is connected to the input link. The ball screw, attached to the input link (Fig. 5d), rotates using a brush-less DC motor. Angular motion of the DC motor is converted to linear motion using a guiding shaft installed at the input link parallel to the ball screw. The distance d (Fig. 1), between the spring housing and the center of rotation can be adjusted using the feedback signal from an encoder installed at the DC motor. A bearing (Fig. 5c) sliding on the output shaft, which is attached to the output link, is pin jointed at the spring

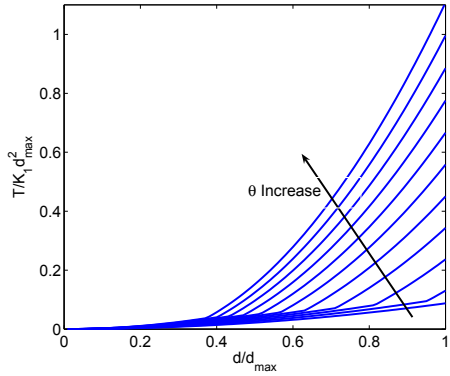

Fig. 2. Effects of increasing $\frac{d}{d_{max}}$ in non–dimensional torque–deformation in RASAT for a constant θ. θ increases in equal steps of 1^o from 5^o to 15^o.

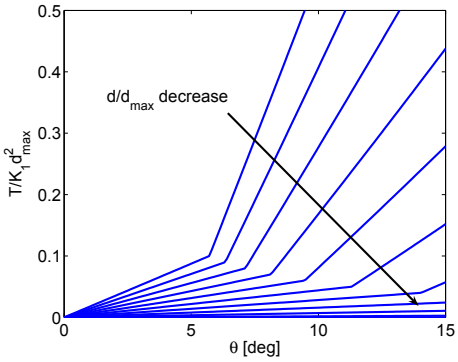

Fig. 3. Each curve shows non–dimensional torque–θ in RASAT for a constant d. $\frac{d}{d_{max}}$ decreases in equal steps of 0.1 from 1 to 0.1.

housing and has sliding motion inside the slot deployed on spring housing. Consequently, with a relative torque between the input and the output links, the bearing slides inside the spring housing and converts the angular motion between the links to the linear motion of the springs. The resultant force caused by the deflection of the springs creates torque through the output shaft via the bearing (Fig. 5c).

2.2 Linear Adjustable Stiffness Artificial Tendon (LASAT)

Linear Adjustable Stiffness Artificial Tendon (LASAT) is an uni–directional compression tendon. LASAT is a series combination of two helical compression springs. A rigid coupler that connects two series springs together is illustrated in Fig. 6. Counterclockwise rotation of the coupler increases the number of active coils in spring 2 with the low stiffness and decreases the number of active coils in spring 1 with the high stiffness; and vice versa for clockwise rotation. Springs 1 and 2 have the stiffnesses of K_{s1} and K_{s2} respectively, which are defined

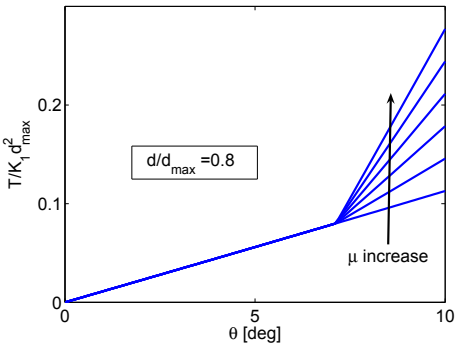

Fig. 4. Effects of increasing μ in non–dimensional torque–θ in RASAT.

by:

$$K_{si} = \frac{P_i}{N_s} \qquad i = 1, 2 \tag{4}$$

where parameter 'i' represents the i^{th} spring and number of spring coils, N_s, is assumed to be equal for both springs. P_1 and P_2 are the coil's stiffness of the spring 1 and 2, respectively (Norton, 1999):

$$P_i = \frac{dia_i^4 G_i}{8 D_i^3} \qquad i = 1, 2 \tag{5}$$

where D_i, dia_i and G_i are the mean coil diameters, wire diameters, the shear modulus of the springs. By changing the position of the coupler, the number of the active coils of spring 1 and spring 2 will be defined by $N_1 = (1 - \lambda)N_s$ and $N_2 = \lambda N_s$ respectively, where $0 < \lambda < 1$. The coil's stiffness of spring 1 is assumed ρ times as high as spring 2, thus $P_1 = \rho P_2$. By the above considerations, the effective stiffness of spring 1, K_{a1}, and the effective stiffness of spring 2, K_{a2}, are given by the following Equations:

$$K_{a1} = \frac{K_{s1}}{1-\lambda} \tag{6}$$

$$K_{a2} = \frac{K_{s2}}{\lambda} \tag{7}$$

The resulted stiffness of the series springs, K_{eq}, represents the LASAT stiffness as long as the compression of softer spring is lower than its shut length, Ls, (where the coils are in contact) that is given below:

$$K_{eq} = \frac{K_{a1}K_{a2}}{K_{a1} + K_{a2}} = \frac{\frac{P_1}{(1-\lambda)N_s}\frac{P_2}{\lambda N_s}}{\frac{P_1}{(1-\lambda)N_s} + \frac{P_2}{\lambda N_s}} = \frac{\rho K_{s2}}{1 + (\rho - 1)\lambda} \tag{8}$$

Thus, the force of the tendon is calculated by the following Equations:

$$F_{LASAT} = \begin{cases} K_{eq} d_{LASAT} & d_{LASAT} \leq Ls\frac{1+(\rho-1)\lambda}{\rho} \\ K_{s2}Ls + K_{a1}(d_{LASAT} - Ls\frac{1+(\rho-1)\lambda}{\rho}) & d_{LASAT} > Ls\frac{1+(\rho-1)\lambda}{\rho} \end{cases} \tag{9}$$

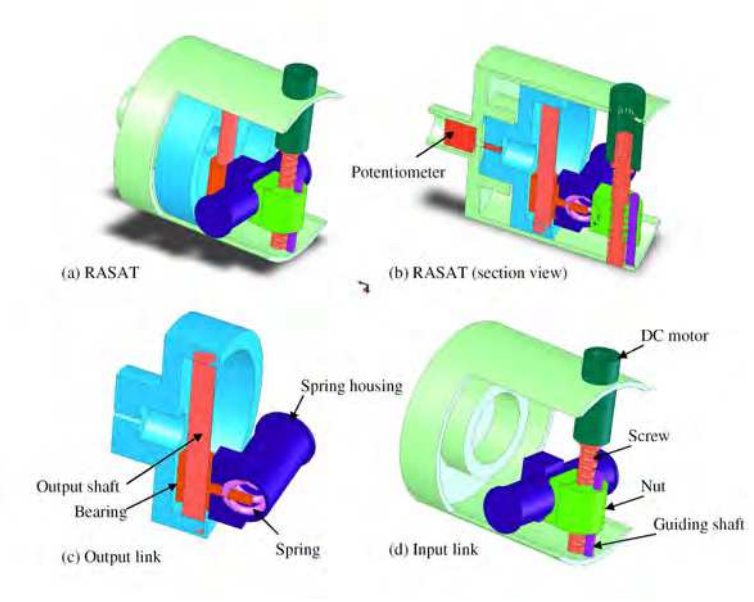

Fig. 5. 3D model of RASAT.

and respectively in its dimension-less form:

$$\frac{F_{LASAT}}{K_{s2}Ls} = \begin{cases} \frac{d_{LASAT}\rho}{Ls(1+(\rho-1)\lambda)} & \frac{d_{LASAT}}{Ls} \leq \frac{1+(\rho-1)\lambda}{\rho} \\ 1+\frac{\rho}{1-\lambda}\left(\frac{d_{LASAT}}{Ls}-\frac{1+(\rho-1)\lambda}{\rho}\right) & \frac{d_{LASAT}}{Ls} > \frac{1+(\rho-1)\lambda}{\rho} \end{cases} \tag{10}$$

where d_{LASAT} is the deflection of the LASAT and the length $Ls\frac{1+(\rho-1)\lambda}{\rho}$ is the total deflection of the tendon at the instance that spring 2 reaches to the shut length. Fig. 7 illustrates the relationship of the dimension-less resultant stiffness of the LASAT, $\frac{K_{eq}}{K_{s2}}$, to the λ (the ratio of the number of active coils of spring 2 to N_s) for different values of ρ (the ratio of the coil stiffness of the spring 1 to the spring 2). In Fig. 7, each curve corresponds to a constant ρ and the value of ρ increases from 1 to 5 with increments of one. As shown, by increasing λ from zero to one for a constant ρ, the resulted stiffness of LASAT, K_{eq}, decreases.

Fig. 8 shows the relation of dimension-less force index $\frac{F_{LASAT}}{K_{s2}Ls}$, to the dimension-less deflection index $\frac{d_{LASAT}}{Ls}$, when $\rho = 5$ as well as λ varies from 0.1 to 0.9 with equal steps of 0.1. As shown in Fig. 8, there is a discontinuity in the slope of each curve as $\frac{F_{LASAT}}{K_{s2}Ls} = 1$ that is caused by the shut length of spring 2. The slope of the curves before the shut length shown in Equation 8 equals to $\frac{\rho}{1+(\rho-1)\lambda}$. The slope after the shut length equals to $\frac{\rho}{1-\lambda}$. By increasing λ, the slope of each curve before the shut length decreases that is resulted to the softer equivalent spring. On the other hand, the slope of the curve after the shut length increases. In general, helical springs are not acting linearly close to their the shut lengths. Thus, to reduce nonlinear effects on the tendon caused by coil contact and friction at the shut length, the LASAT should be designed in a way to prevent reaching the shut length.

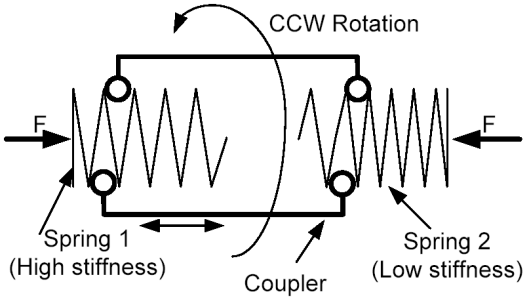

Fig. 6. Schematic of LASAT.

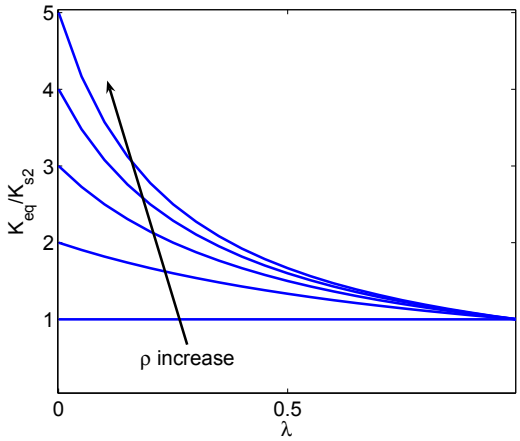

Fig. 7. Non–dimensional relation of stiffness–λ in LASAT before shut length. Each curve corresponds to a constant ρ while ρ increases from 1 to 5 with steps of 1.

From the mechanical design point of view, LASAT is comprised of an input rod, an output rod, two springs and a spring positioning mechanism as shown in Fig. 9. The springs can slide inside the output rod and have the same coil pitch and the mean diameter, but have different wire diameters. The inner diameter of the output rod is assumed to be smaller in the area that contacts with the softer spring than in the area that contacts with the stiffer spring. The output force is directly applied to the low stiffness spring and a notch inside the output rod makes a stopper that prevents the softer spring from reaching to the shut length. The positioning mechanism of the coupler consists of a brush-less DC motor, a spline shaft and a coupling element. The outer surface of the coupler is screw threaded with the lead equal to the spring's coil pitch. The inner surface of the coupler holds a ball spline bush which slides over the spline shaft freely (as shown in Fig. 9). The rotation of the spline shaft by brush-less DC motor transfers to the coupling element by the ball spline. Therefore, the angular motion of the coupling element converts to linear motion and simultaneously changes the number of

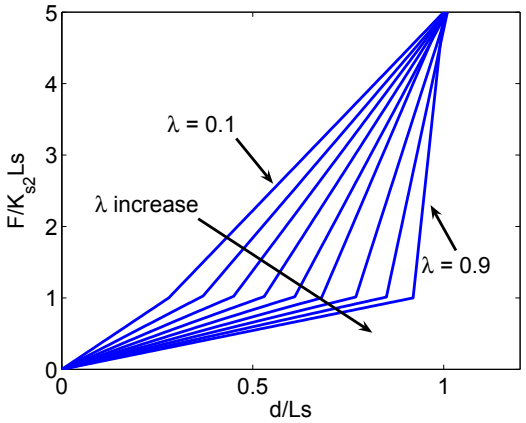

Fig. 8. Non–dimensional graph of force–deformation in LASAT. Sudden changes in slopes of the curves are caused by shut length of spring 2.

the spring coils in each spring. Also, an encoder is installed on the brush-less DC motor to measure the location of the coupling element.

2.3 Offset Location Adjustable Stiffness Artificial Tendon (OLASAT)

The Offset Location Adjustable Stiffness Artificial Tendon (OLASAT) is specially designed to switch the stiffness between two specific values. Here, the artificial tendon is a combination of two parallel springs (spring 1 and spring 2) placed with an offset. As shown in Fig. 10, the offset, a, is the distance between the end points of two springs when the springs are in their neutral lengths. By adjusting the offset using a linear actuator, the deformation requirement which engages spring 2 is changed. The applied force, F_{OLASAT}, of the tendon is a function of the stiffness of spring 1 with a low stiffness (K_{sp1}), spring 2 with a high stiffness (K_{sp2}), the offset (a) and the spring's deflection (d_{OLASAT}) as follows:

$$F_{OLASAT} = \begin{cases} K_{sp1} d_{OLASAT} & d_{OLASAT} < a \\ K_{sp1} a + (K_{sp1} + K_{sp2})(d_{OLASAT} - a) & d_{OLASAT} \geq a \end{cases} \tag{11}$$

The above equation in the dimensionless form appears in Equation(12) where K_{sp2} is replaced by ηK_{sp1}.

$$\frac{F_{OLASAT}}{K_{sp1} a} = \begin{cases} \frac{d_{OLASAT}}{a} & \frac{d_{OLASAT}}{a} < 1 \\ 1 + (1+\eta)(\frac{d_{OLASAT}}{a} - 1) & \frac{d_{OLASAT}}{a} \geq 1 \end{cases} \tag{12}$$

The force-deflection graph of the OLASAT is illustrated in Fig. 11. η is the ratio of the stiffness of spring 2 to that of spring 1 ($\eta = 5$ in Fig. 11). The slopes of the straight lines in Fig. 11 represent the stiffness of OLASAT. The stiffness is suddenly switched from the stiffness of spring 1, K_{sp1}, to the stiffness of two parallel springs, $(\eta + 1)K_{sp1}$, at point $d_{OLASAT} = a$.
From the mechanical design point of view, OLASAT is a uni-directional tendon and consists of an input rod, an output rod, a low stiffness spring and a high stiffness spring, with a positioning mechanism using a ball screw and a nut (as shown in Fig. 12). The low stiffness

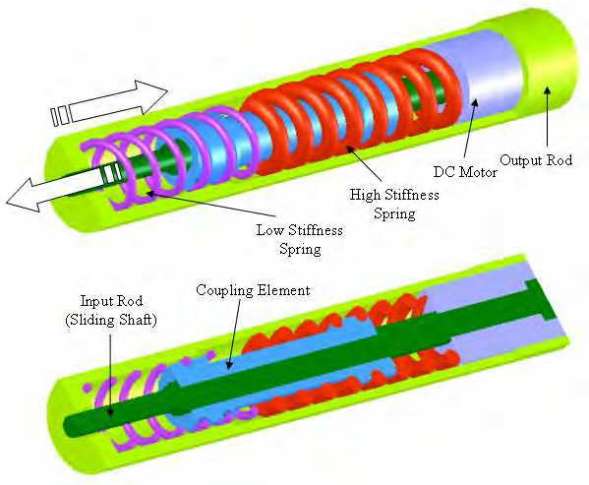

Fig. 9. 3D model of LASAT.

spring is coupled between the input and output rods. The high stiffness spring is connected to the input rod on one side and is free on the other side. A miniature brushless DC motor connected to the ball screw provides the sliding motion of the high stiffness spring over the slot deployed on the input rod, which can adjust the offset between the two springs.

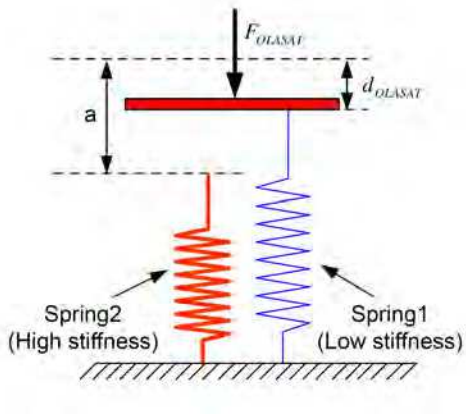

Fig. 10. Schematic of the OLASAT.

3. Bipedal walking gait in the simplified model

A simplified model and the gait cycle of a bipedal walking robot are introduced here. The model offers different advantages. It is simple, and hence decreases the complexity of analysis in energy economy. In addition, it considers the effects of OLASAT and the foot. It also

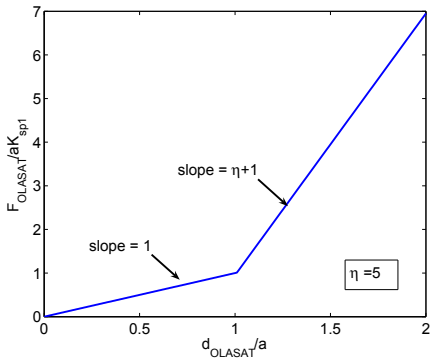

Fig. 11. Non–dimensional force–deformation graph of OLASAT.

includes the double support phase and has the ability to inject energy to the biped. The dynamics of the swing leg is not considered in the model to avoid complexity of the analysis.
In the model, as shown in Fig. 13, a rigid foot with a point mass is pivoted at the ankle joint to a rigid stance leg with a lumped mass at the hip (upper tip of the stance leg). One end of OLASAT is attached to the stance leg and the other end is attached to the foot. A cable and pulley mechanism converts the angular movement of the ankle joint to the linear deformation of the springs in OLASAT. The model also includes a massless linear spring to simulate the force of the trailing leg during the double support stance phase. The linear spring injects the energy to the biped. The input energy through the spring of the trailing leg can be adjusted by either controlling the initial deformation of the spring or adjusting its stiffness. However in this work , only the effects of the stiffness adjustment of OLASAT are studied in the simulation results and the stiffness of the trailing leg spring is taken zero. To simplify the analysis, planar motion and friction-free joints are assumed in the bipedal walking model.
In general, as shown in Fig. 14, the stance phase includes (in both single and double support periods) the collision, the rebound and the preload phases. The collision phase starts with the impact of the heel-strike followed by continuous motion. At the end of the collision, a second impact of the foot-touch-down occurs. Both impacts are assumed to be rigid to rigid, instantaneous and perfectly plastic, which dissipates part of the energy of the biped. In this model, the offset between the two springs of OLASAT, as shown in Fig. 10, can be adjusted to store part of the energy of the biped during the continuous motion of the collision phase and to reduce the impact at the foot-touch-down. The offset is adjusted only once during the swing phase while there is no external load on the foot. Then it remains constant for the following supporting period. The second phase, rebound, is a continuous motion while the foot is assumed stationary on the ground. The stored energy in OLASAT during the collision phase returns to the biped during the rebound phase. The rebound phase ends at midstance (biped upright position). OLASAT is passively loaded during the collision phase and is passively unloaded during the rebound phase. The motion of the biped after midstance is named the preload phase which continues until the heel-strike of the following walking step (Kuo et al., 2005). The kinematics of the heel-strike of the following walking step is specified by step length and the geometry of the robot.
The bipedal walking model in this work consists of a pre-deformed compression linear spring to simulate the force of the trailing leg. The linear spring of the trailing leg is massless with

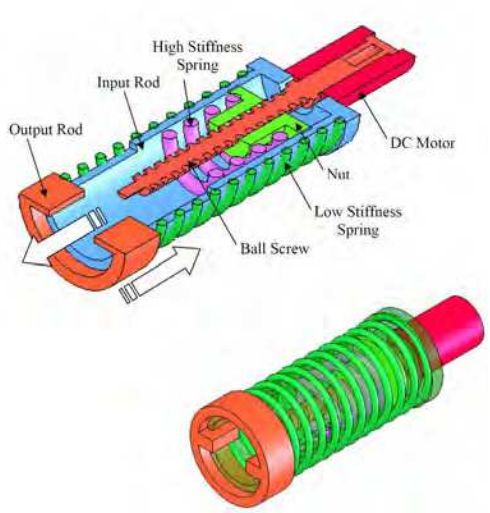

Fig. 12. 3D model of OLASAT.

one end connected to the toe of the foot on the ground and the other to the upper tip of the stance leg as shown in Fig. 13. It is also shown in Fig. 14 by B. The force vector from the compliant trailing leg (F in Fig. 14) is applied on the upper tip of the stance leg until the spring reaches its relaxed length (determining the end of the double support phase). By assuming the trailing leg as an elastic element, the model provides several advantages. The simplicity of dynamic modeling and analysis during impact events and the capability of injecting the external energy are two major advantages.

3.1 Dynamic model of the bipedal walking

The details of the dynamic modeling of the proposed bipedal walking model are given in (Ghorbani, 2008). In this section, the parameters of the simplified model of the bipedal walking on level ground are presented. In Fig. 13, links 1 and 2 are the foot and the stance leg. The values of d_1 and d_2 represent the distance between the center of mass of the foot to the heel and that of the body to the ankle joint respectively. l_1 is the distance between the heel and the ankle joint. l_2 is the distance between the ankle joint and the center of mass of the body which is at the upper end of the stance leg. Thus in the model, $l_2 = d_2$. θ_1 and θ_2 are denoted as the angles of the foot and the stance leg with respect to the horizontal axis as illustrated in Fig. 13. x_h and y_h represent the horizontal and vertical distance between the heel and a reference point O on the ground. In this work, the origin O is defined at the heel of the stance leg. The dimensionless parameters of the model are specified and listed in Table 1. Generalized coordinates of the biped are the horizontal and vertical positions of the heel as

Parameters	β	ψ	ζ	υ	ς	η	ν
Equivalence	$\frac{m_1}{m_2}$	$\frac{l_1}{l_2}$	$\frac{d_1}{l_2}$	$\frac{l_t}{l_2}$	$\frac{K_1R^2}{m_2l_2g}$	$\frac{K_2}{K_1}$	$\frac{K_tl_2}{m_2g}$

Table 1. Dimensionless Parameters.

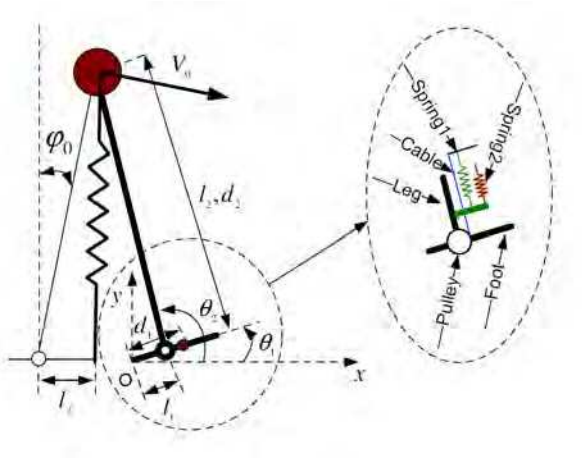

Fig. 13. Bipedal walking model schematic.

well as foot and stance leg angles with respect to the horizontal line which correspond to x_h, y_h, θ_1 and θ_2, respectively. The perpendicular position of the foot to the stance leg is assumed as a neutral position (no force) of OLASAT in this work. The heel is assumed to be pivoted to the ground during the collision phase by assuming enough friction force between the foot and the ground. Dynamic modeling of the bipedal walking, which is detailed in (Ghorbani, 2008), includes the heel-strike, the continuous motion during the collision phase as well as the rebound and the preload phases. The equations of motion in the normalized form with dimensionless parameters can help one to study more efficiently the bipedal walking motion in a generalized form. It also assists in the parametric follow-up study. The section 3.2 presents the normalized form of the equations of motion.

3.2 Equations of motion in normalized form

The dimensionless parameters of the model are specified and listed in Table 1. The equations of motion are normalized by $m_2 l_2^2$, the inertia of the stance leg about the ankle joint. Finally, by replacing the dimensionless parameters into the normalized form of the equations of motion, the normalized form of the equations of motion are arrived at. The normalized form of the dynamics equation at the heel-strike appears below.

$$\begin{bmatrix} \frac{\beta+1}{l_2^2} & 0 & \frac{\beta\zeta+\psi\sin(\theta_1)}{l_2} & \frac{1}{l_2} \\ 0 & \frac{\beta+1}{l_2^2} & \frac{\beta\zeta+\psi\cos(\theta_1)}{l_2} & \frac{1}{l_2} \\ \frac{\beta\zeta+\psi\sin(\theta_1)}{l_2} & \frac{\beta\zeta+\psi\cos(\theta_1)}{l_2} & \beta\zeta^2+\psi^2 & \psi\cos(\Delta\theta) \\ \frac{1}{l_2} & \frac{1}{l_2} & \psi\cos(\Delta\theta) & 1 \end{bmatrix} \begin{bmatrix} {}_{-}{}^{HS}\dot{x}^{-} \\ {}_{-}{}^{HS}\dot{y}^{-} \\ {}^{HS}(\dot{\theta}_1^{+}-\dot{\theta}_1^{-}) \\ {}^{HS}(\dot{\theta}_2^{+}-\dot{\theta}_2^{-}) \end{bmatrix} = \begin{bmatrix} \frac{{}^{HS}\hat{\lambda}_1}{m_2 d_2^2} \\ \frac{{}^{HS}\hat{\lambda}_2}{m_2 d_2^2} \\ 0 \\ 0 \end{bmatrix} \tag{13}$$

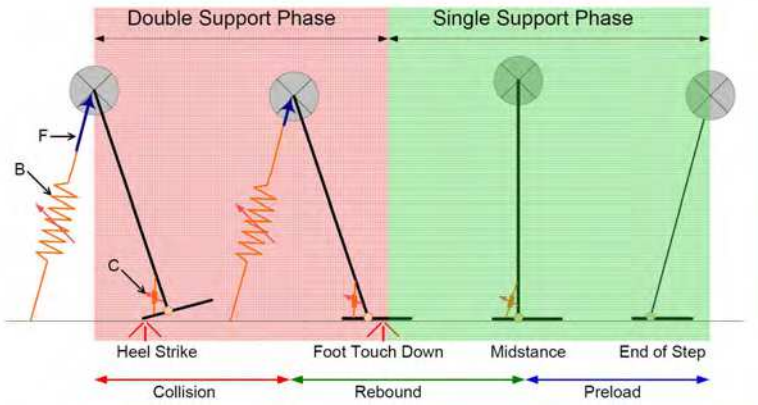

Fig. 14. General Schematic of the bipedal gate.

where $\Delta\theta = \theta_1 - \theta_2$. The normalized form of the equations of motion at the foot-touch-down is

$$\begin{bmatrix} \beta\zeta^2 + \psi^2 & \psi\cos(\Delta\theta) \\ \psi\cos(\Delta\theta) & 1 \end{bmatrix} \begin{bmatrix} -\,{}^{FTD}\dot{\theta}_1^- \\ {}^{FTD}(\dot{\theta}_2^+ - \dot{\theta}_2^-) \end{bmatrix} = \begin{bmatrix} \frac{{}^{FTD}\hat{\lambda}}{m_2 d_2^2} \\ 0 \end{bmatrix} \tag{14}$$

Equation (15) is the normalized counterpart of Equation.

$$\hat{M}(\theta)\ddot{\theta} + \hat{H}(\theta,\dot{\theta})\dot{\theta} + \hat{G}(\theta) + \hat{S}(\theta) = \hat{I}(\theta) \tag{15}$$

where

$$\hat{M} = \begin{bmatrix} \beta\zeta^2 + \psi^2 & \psi\cos(\Delta\theta) \\ \psi\cos(\Delta\theta) & 1 \end{bmatrix} \tag{16}$$

$$\hat{H} = \begin{bmatrix} 0 & \psi\sin(\theta_2 - \theta_1)\dot{\theta}_2 \\ \psi\sin(\theta_2 - \theta_1)\dot{\theta}_1 & 0 \end{bmatrix} \tag{17}$$

$$\hat{G} = \begin{bmatrix} \frac{\beta\zeta+\psi}{l_2} g\cos(\theta_1) \\ \frac{g}{l_2}\cos(\theta_2) \end{bmatrix} \tag{18}$$

$$\hat{S} = \frac{\varsigma}{l_2} \begin{bmatrix} -g(\Delta\theta - \frac{\pi}{2}) - \gamma\eta g(\Delta\theta - \frac{\pi}{2} - a/R) \\ g(\Delta\theta - \frac{\pi}{2}) + \gamma\eta g(\Delta\theta - \frac{\pi}{2} - a/R) \end{bmatrix} \tag{19}$$

$$\hat{I} = \begin{bmatrix} -\frac{\iota\nu g(L_0 - L_t)\beta}{l_2^2}\sin(\theta_1)\cos(\delta) + \frac{\iota\nu g(L_0 - L_t)\beta}{l_2^2}\cos(\theta_1)\sin(\delta) \\ -\frac{\iota\nu g(L_0 - L_t)\beta}{l_2^2}\sin(\theta_2)\cos(\delta) + \frac{\iota\nu g(L_0 - L_t)\beta}{l_2^2}\cos(\theta_2)\sin(\delta) \end{bmatrix} \tag{20}$$

The equations of motion during rebound is

$$\ddot{\theta_2} + \frac{g}{2}\cos(\theta_2) + \varsigma\frac{g}{l_2}(\theta_2 - \frac{\pi}{2}) + \gamma\eta\varsigma\frac{g}{l_2}(\theta_2 - \frac{\pi}{2} - \frac{a}{R}) \tag{21}$$
$$= -\frac{\iota\nu g(L_0 - L_t)\beta}{l_2^2}\sin(\theta_2)\cos(\delta) + \frac{\iota\nu g(L_0 - L_t)\beta}{l_2^2}\cos(\theta_2)\sin(\delta)$$

The next section presents the calculations related to energy loss during the foot-touch-down, which is the major source of energy loss in the proposed bipedal walking model.

4. Discussion of the energy loss

The energy loss during the foot-touch-down is one of the major causes of energy reduction in bipedal walking which is reduced by properly adjusting the stiffness of OLASAT. This section studies the key parameters involved in the change in the kinetic energy of the biped, ${}^{FTD}\Delta E = {}^{FTD}E^- - {}^{FTD}E^+$, before and after the foot-touch-down, shedding light on how the stiffness adjustment of OLASAT can reduce the energy loss. ${}^{FTD}\Delta E$ for the model explained in Fig. 13 is given below.

$${}^{FTD}\Delta E = 0.5m_2l_2^2(({}^{FTD}\dot{\theta}_2^-)^2 - ({}^{FTD}\dot{\theta}_2^+)^2) + 0.5(m_1d_1^2 + m_2l_1^2)({}^{FTD}\dot{\theta}_1^-)^2 \tag{22}$$
$$+m_2l_1l_2\cos({}^{FTD}\theta_2)({}^{FTD}\dot{\theta}_1^-)({}^{FTD}\dot{\theta}_2^-)$$

On the other hand ${}^{FTD}\dot{\theta}_2^+$ is calculated from the equation of motion detailed in (Ghorbani, 2008)

$${}^{FTD}\dot{\theta}_2^+ = {}^{FTD}\dot{\theta}_2^- + \frac{l_1\cos(\theta_2 - \theta_1)\ {}^{FTD}\dot{\theta}_1^-}{d_2} \tag{23}$$

By substituting of ${}^{FTD}\dot{\theta}_2^+$ from Equation (23) into Equation (22) and after simplification, the following relation is obtained.

$${}^{FTD}\Delta E = 0.5(m_1d_1^2 + m_2l_1^2\sin^2({}^{FTD}\theta_2^-))({}^{FTD}\dot{\theta}_1^-)^2 \tag{24}$$

Masses, lengths of the links and $\sin^2({}^{FTD}\theta_2)$ are all positive. Equation (24) illustrates the direct relation of ${}^{FTD}\Delta E$ with $({}^{FTD}\dot{\theta}_1^-)^2$. It indicates that reducing the magnitude of the angular velocity of the foot immediately before the foot-touch-down can significantly reduce the energy loss of the biped. In addition, Equation (23) illustrates the direct relation of ${}^{FTD}\dot{\theta}_2^+ - {}^{FTD}\dot{\theta}_2^-$ with ${}^{FTD}\dot{\theta}_1^-$ which indicates that by reducing the magnitude of ${}^{FTD}\dot{\theta}_1^-$ the change of angular velocity of the stance leg at the foot-touch-down is reduced.
By taking the time derivative of the position of the center of mass (COM) of the body, ${}^{FTD}Y_{COM}^-$, its velocity is arrived at as given below:

$${}^{FTD}\dot{Y}_{COM}^- = l_1\ {}^{FTD}\dot{\theta}_1^- + l_2\ {}^{FTD}\dot{\theta}_2^-\cos({}^{FTD}\theta_2) \tag{25}$$

${}^{FTD}\dot{\theta}_2^-$ and $\cos({}^{FTD}\theta_2)$ are negative before midstance. The optimum situation ${}^{FTD}\Delta E = 0$ can be achieved by reducing $({}^{FTD}\dot{\theta}_1^-)^2$ to zero. In such a scenario, the velocity of the COM of the body at the foot-touch-down will be upward. This indicates that the direction of the velocity vector of the COM of the body at the heel-strike ${}^{HS}\dot{Y}_{COM}^-$, which is downward, should be reversed to the upward direction at the foot-touch-down during the collision phase to reduce

the energy loss. This is made possible by storing part of the kinetic energy of the biped in elastic form during the collision phase. This notion can be reinforced in human walking. Donelan expressed that humans redirect the center of mass velocity during step-to-step transitions not with instantaneous collisions, but with negative work performed by the leading leg over a finite period of time (Donelan & Kuo, 2002; Donelan et al., 2002). These findings serve as the foundation to determine the offset of OLASAT. As a result, the development of an automatic controller to adjust the stiffness of OLASAT is necessary to improve the performance of the bipedal walking which is described in the following section.

5. Design of the stiffness adjustment controller

In general, OLASAT has two major roles during the collision phase. The first role is to compensate the moment about the ankle joint exerted by the gravitational force of the body. The second is to store part of the kinetic energy of the biped. Both of these two roles can reduce $({}^{FTD}\dot{\theta}_1^-)^2$. This section provides a guideline for determining the offset of OLASAT, a, in order to store part of the energy of the biped, thus reducing $({}^{FTD}\dot{\theta}_1^-)^2$, and consequently reducing the energy loss. The development of a controller to satisfy such an optimal condition of $({}^{FTD}\dot{\theta}_1^-)^2 = 0$ can be possible by predicting the dynamics of the bipedal walking in advance. On the other hand, perfectly predicting the dynamics of the biped is not realistic because of the complexity of physical robots. Thus, a controller is developed in this section to estimate the offset of OLASAT without requiring the full knowledge of the system dynamics. To design such a controller, the following assumptions are made in this work.

First, OLASAT is loaded and unloaded passively during the stance phase. Thus for the following walking step, the offset is adjusted during the swing phase of the current walking step while the foot is not in contact with the ground. Second, the feedback signals of the biped are taken to be the angular position, θ_2, and the angular velocity, $\dot{\theta_2}$, of the stance leg. The reason for specifying these two signals as feedback is that the biped is an inverted pendulum during the rebound and the preload phases. Thus, the velocity of the biped at the heel-strike of the following walking step can be determined from the angular velocity of the stance leg at midstance, ${}^{MD}\dot{\theta}_2$. This choice allows enough time to adjust the offset during the swing phase which is important from the practical point of view. Third, the foot is perpendicular to the stance leg immediately before the heel-strike and in such a situation, OLASAT is in the neutral position (with no force). Fourth, the step length is fixed by assuming that the swing leg is perfectly controlled. Fifth, the angular displacement of the stance leg relative to the ground is negligible during the collision phase. This assumption results in the approximation of ${}^{FTD}\theta_2^- = {}^{HS}\theta_2^-$. It ensures that the total deformation of spring 1 in OLASAT is equal to $R\,{}^{HS}\theta_1^-$. ${}^{HS}\theta_1^-$ and ${}^{HS}\theta_2^-$ are the θ_1 and θ_2 immediately before the heel-strike which are known from the walking step length.

The stiffness adjustment controller developed here determines the offset of OLASAT, a, which corresponds to the angular offset of $\frac{a}{R}$ at the pulley of the ankle joint. Here, the maximum angular displacement of the pulley ($\Delta\vartheta$), in which spring 2 is engaged during the collision phase, is determined first to calculate the offset. Before determining the offset, we first discuss the selection of the stiffness of spring 1 of OLASAT. The stiffness of spring 1 must be selected low enough to prevent the leg from bouncing during the collision phase even for minimum bipedal walking speed while spring 2 is not engaged (minimum stiffness of OLASAT). It must also be selected high enough to compensate a portion of the gravitational moment about the ankle joint at the foot-touch-down and also to store part of the kinetic energy of the biped. Next, we explain the procedure of determining $\Delta\vartheta$.

$\Delta\vartheta(n+1)$ is calculated from the feedback loop of the stiffness adjustment controller for the walking step n+1. Walking step n is started from the heel-strike which includes the double support phase and will end immediately before the heel-strike of the step n+1. The inputs of the stiffness adjustment controller are the angular velocity of the stance leg at midstance, ${}^{MD}\dot{\theta}_2(n)$, of the current walking step n, and the stiffness of the trailing leg spring of the following walking step, $K_t(n+1)$. The output of the stiffness adjustment controller is the offset of OLASAT for the walking step n+1. $K_t(n+1)$ can be determined using a speed tracking controller to inject energy to the biped which is not discussed in this work and further information is referred to (Ghorbani, 2008).

Part of the kinetic energy of the biped at the end of the walking step n is stored in the trailing leg spring during the collision phase of the walking step n+1. Based on the results obtained in Section 4, the OLASAT should also store part of the kinetic energy during the collision phase of the walking step n+1. Here, the elastic potential energy, $0.5K_{sp2}R^2(\Delta\vartheta(n+1))^2$, of the walking step n+1 stored in spring 2 is assumed to be proportional to the difference between the kinetic energy of the biped at the end of the walking step n, $0.5m_2(l_2\ {}^{EN}\dot{\theta}_2^-(n)\sin(\varphi_0(n)))^2$, associated with the vertical component of the velocity of the COM of the body, and the elastic potential energy of trailing leg spring, $\frac{1}{2}K_t(\Delta L_{col}^2 - \Delta L_{dss}^2)$, during the collision phase of the walking step n+1 where $\varphi_0(n) = \frac{\pi}{2} - {}^{EN}\theta_2^-(n)$. ${}^{EN}\theta_2^-(n)$ and ${}^{EN}\dot{\theta}_2^-(n)$ are the angle and the angular velocity of the stance leg at the end of the preload phase of the walking step n. ΔL_{dss} and ΔL_{col} are the deformation of the tailing leg spring at the heel-strike and the deformation of the tailing leg spring at the foot-touch-down of the walking step n+1. The following equation describes the above energy relation.

$$\frac{1}{2}K_{sp2}R^2(\Delta\vartheta(n+1))^2 = \frac{1}{2}K_{adjust}(m_2(l_2\ {}^{EN}\dot{\theta}_2^-(n)\sin(\varphi_0(n)))^2 - K_t(n+1)(\Delta L_{col}^2 - \Delta L_{dss}^2)) \tag{26}$$

K_{adjust} is a proportional gain and $\Delta L_{col} = L_0 - {}^{FTD}L_t$, where ${}^{FTD}L_t$ is the length of the trailing leg spring at the foot-touch-down of the walking step n+1 which can be calculated from the kinematics of the biped using the following assumptions. Here, the stiffness of the trailing leg should be limited preventing the right hand side of Equation (26) from having a negative value. The step length and the initial angles of the foot and the stance leg for the walking step n+1 are known values in this work. Preload is also assumed as a free rotating inverted pendulum under gravity. ${}^{EN}\dot{\theta}_2^-(n)$ can be calculated from the angular velocity of the leg at midstance, ${}^{MD}\dot{\theta}_2(n)$, using the following energy relation:

$$0.5m_2l_2^2({}^{EN}\dot{\theta}_2^-(n))^2 = 0.5m_2l_2^2({}^{MD}\dot{\theta}_2^2(n)) + m_2gl_2(1-\cos(\varphi_0(n))) \tag{27}$$

The first term in the right-hand side of the above relation is the kinetic energy of the biped at midstance of the walking step n which is measurable from the feedback signals. It is assumed that the double support phase is ended before the midstance. Thus the injected energy, through the trailing leg spring during the double support phase of the walking step n, is converted to the kinetic energy of the biped which is measured at the midstance. The second term of the right-hand side of Equation (27) is the change in the gravitational potential energy of the biped between the midstance of the walking step n and the heel-strike of the walking step n+1 which can be calculated by assuming a fixed amount for the step length. By calculating ${}^{EN}\dot{\theta}_2^-(n)$ from Equation (27), which results in ${}^{EN}\dot{\theta}_2^-(n) = \sqrt{{}^{MD}\dot{\theta}_2^2(n) + \frac{2g}{l_2}(1-\cos(\varphi_0(n)))}$,

and by substituting it into Equation (26), $\Delta\vartheta(n+1)$ is determined to be as follows.

$$\Delta\vartheta(n+1) = \sqrt{\frac{K_{adjust}}{R^2 K_{sp2}}}\sqrt{m_2(l_2\ {}^{EN}\dot{\theta}_2^-(n)\ \sin(\varphi_0(n)))^2 - K_t(n+1)(\Delta L_{col}^2 - \Delta L_{dss}^2)} \quad (28)$$

Finally, as mentioned above by assuming that the angular movement of the stance leg relative to the ground is negligible during the collision phase, the offset $\frac{a}{R}(n+1)$ is calculated from the relation below.

$$\frac{a}{R}(n+1) = {}^{HS}\theta_1^-(n+1) - \Delta\vartheta(n+1) \quad (29)$$

The next section presents the simulation results of the bipedal walking motion in different case studies.

6. The study of energetics through simulations

The effects of the adjustable stiffness artificial tendon on the energetics of bipedal walking is studied in this section through computer simulations. In section 6.1, the simulation results of bipedal walking are illustrated during the single support phase for a single walking step. The simulation results show significant improvement in reducing the energy loss by proper adjustment of the stiffness of OLASAT. Then, the simulation results of the robot during single support phase are presented for 5 consecutive walking steps in section 6.2 to compare the results of the two cases of the single spring with best selected stiffness and OLASAT with the well-adjusted stiffness. Finally the controller developed in section 5 is implemented to automatically adjust the offset of OLASAT for reducing energy loss during the collision phase.

6.1 Stance phase of bipedal walking during a single walking step

In this section, a realization of the single support phase of bipedal walking is demonstrated for two different cases of a single spring and OLASAT during a single walking step. The stiffness of the single spring equals the stiffness of the spring 1 in OLASAT. Here, the stiffness of spring 1 in OLASAT is defined through trial and error. The objective was to find a stiffness which prevents the leg bouncing at the FTD for wide range of initial velocities, and which is high enough to store the elastic energy during the collision phase. In order to study the effects of stiffness adjustment on the energy economy of the biped, simulations are performed for the same initial conditions for both cases.

The parameters of the biped in computer simulations are listed in Table 2 in addition to $m_2 = 1kg$ and $l_2 = 1.0m$. The initial conditions of the biped immediately before the heel-strike in

Parameters	β	ψ	ζ	υ	ς	η
Value	0.02	0.05	0.07	0.1	0.5	4

Table 2. Dimensionless Parameters of the simulations.

the simulation are specified as follows: ${}^{HS}\theta_1^- = 15^o$, ${}^{HS}\theta_2^- = 105^o$, $x_h = y_h = 0$, ${}^{HS}\dot{\theta}_1^- = {}^{HS}\dot{\theta}_2^- = 0$ and $\varphi_0 = 11.7^o$. The initial translational velocity V_0 of the biped before the heel-strike has the magnitude of $1.5m/s$ with the horizontal angle of $-\varphi_0$.

Using those initial conditions, the total kinetic energy of the biped before the heel-strike is equal to 1.125 [J]. The stiffness of the trailing leg spring is assumed zero in this section, ($\nu = 0$), to simulate the biped's motion with no external elastic energy input. Note that the dynamics

of the swing leg is not assumed in the model.
Fig. 15 shows the simulation results of the biped in case 1 (single spring with best selected stiffness) and case 2 (OLASAT with well-adjusted stiffness). OLASAT's offset value in case 2 is provided using a trial and error procedure, $\frac{a}{R} = 6.0^o$, which reduces the angular velocity of the foot before the foot-touch-down to decrease the energy loss. Fig. 15a shows the joint angles of the biped θ_1, θ_2 which indicate that the motion of the biped is sustained in both cases. Fig. 15b shows the magnitudes of the velocity vector of the COM of the body. As shown in Fig. 15b, the velocity jump of the COM of the body during the FTD in case 2, which equals 0.01 $\frac{m}{sec}$, is significantly lower than case 1, which equals 0.15 $\frac{m}{sec}$. Consequently, the final velocity of the COM of the body is higher in case 2 compared to case 1. These results indicate that the biped can sustain the motion during the stance phase in both cases. Dimensionless kinetic energy κ, is defined as the ratio of the kinetic energy of the biped to its gravitational potential energy at midstance, $m_2 l_2 g$. Fig. 15c depicts the κ versus time, and the comparison of the results indicates that the kinetic energy loss at the FTD is significantly reduced in case 2, that is by 1%, resulting from the proper adjustment of the OLASAT, compared to the κ in case 1 which is as high as 20%. These results illustrate the effects of proper stiffness adjustment of OLASAT on the energetics of the bipedal walking. The significant reduction in energy loss during the FTD in case 2 results in higher final velocity of the body compared to the case 1. The displacement of the COM of the body during the collision phase together with its velocity vector is shown in Fig. 15d. Fig. 15d shows that the vertical component of the velocity of the body's COM is gradually decreased during the collision phase which can reduce the energy loss at the FTD as discussed in Section 4.
The dimensionless parameter of τ_{ankle} is the ratio of the torque of the ankle joint exerted by OLASAT to $m_2 g l_2$ during the single support stance phase. The graph of τ_{ankle} versus time is given in Fig. 16 for the above two cases. The exerted torque by OLASAT in case 1 is much lower than case 2. As shown in Fig. 16, the graphs include different sudden changes of slopes of the τ_{ankle} in the time period of the stance phase. In case 1, this behavior is caused by the end of the collision phase defined by point B and by the end of the rebound phase defined by F. OLASAT performs differently in case 2 while both of the springs are engaged in part of the time period of the motion. At the beginning of case 2, spring 2 is not engaged. After A in Fig. 16, both springs are engaged and they will remain engaged up to D. The change of slope in case 2 at C occures at the end of the collision phase. Point E is also defined by the end of the rebound phase in case 2. Figure 16 indicates that in OLASAT more energy is stored and released during the stance phase. To continue this study, the next section illustrates the effectiveness of adjusting the stiffness of the OLASAT in consecutive walking steps.

6.2 Bipedal walking simulations in consecutive steps

In the last section, a single step of bipedal walking was realized by implementing the OLASAT at the ankle joint. In this section, the simulation results of the bipedal walking in consecutive steps are presented. The goal is to demonstrate and quantify the effects of adjusting the stiffness of the ankle joint on multiple steps of the bipedal walking. During consecutive walking, a gravitational energy of the mass of the foot is injected to the biped caused by leg's initial angle in each walking step. For the first walking step, the same biped configuration and the same initial conditions as in Section 6.1 are used. The biped is moving on level ground. To demonstrate the kinetic energy loss of the biped in this section, $\Delta\kappa_n$ is defined as the dimensionless ratio of the total kinetic energy loss of the biped after n walking steps to the gravitational potential energy of the biped, $m_2 g l_2$, at midstance.

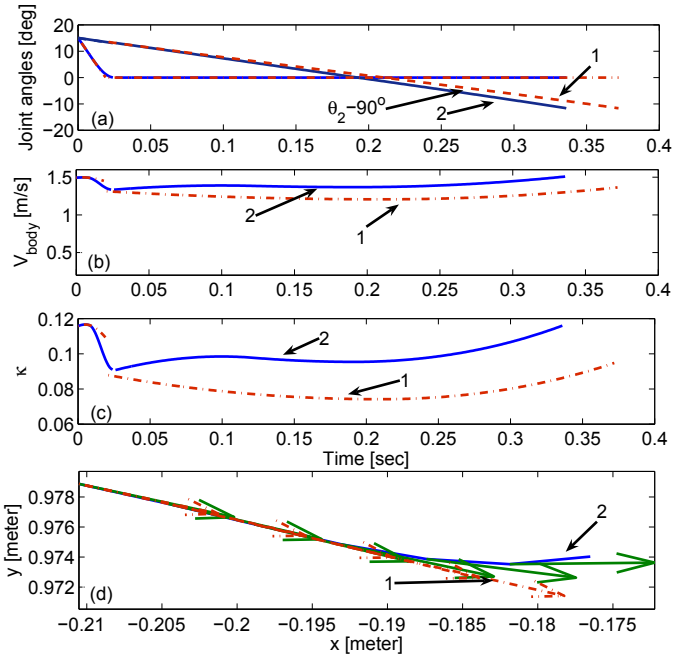

Fig. 15. Simulation results during the single support stance period for both cases of single spring, case1, and OLASAT with well-adjusted stiffness, case 2. (a)- Joint angles vs. time. (b)- Velocity of COM of the body vs time. (c)- Dimensionless kinetic energy of the biped vs time. (d)- Position and velocity vector of COM of the body during the collision phase.

Fig. 17 illustrates the velocity of the COM of the body in 5 consecutive walking steps. It also demonstrates that the motion of the biped is sustained in all steps for all cases. For the case of a single spring, it shows how stepping forward increases the period of each walking step. Reducing the average velocity of the biped is caused by the energy loss of the impact events. On average, for the single spring with the bests stiffness, 8% of the kinetic energy of the biped is dissipated in each step and $\Delta\kappa_5 = 0.0892$. For the case of OLASAT the changes in the step period and velocity of the COM of the body are insignificant as compared with those for the case of the single spring. On average in this case, 0.5% of the kinetic energy of the biped is dissipated in each walking step when $\Delta\kappa_5 = 0.0527$. These results show how the OLASAT, with ability of proper adjustment of the stiffness, significantly improves the energetics of the biped and makes it more efficient. This justifies the developement of an automated stiffness adjustment controller.

Fig. 17 also illustrates the velocity of the COM of the body in 5 consecutive walking steps while the stiffness of OLASAT is adjusted automatically, explained in Section 5. In order to simulate the well-adjusted stiffness, $\frac{a}{R}$ is assumed to be 6.0^o in the first walking step. The proportional gain of the automated stiffness adjustment controller, K_{adjust}, can play an important role in optimally adjusting the offset. Optimal iteration procedure to obtain the best gain remains as future research. Through trial and error simulations, it has been observed

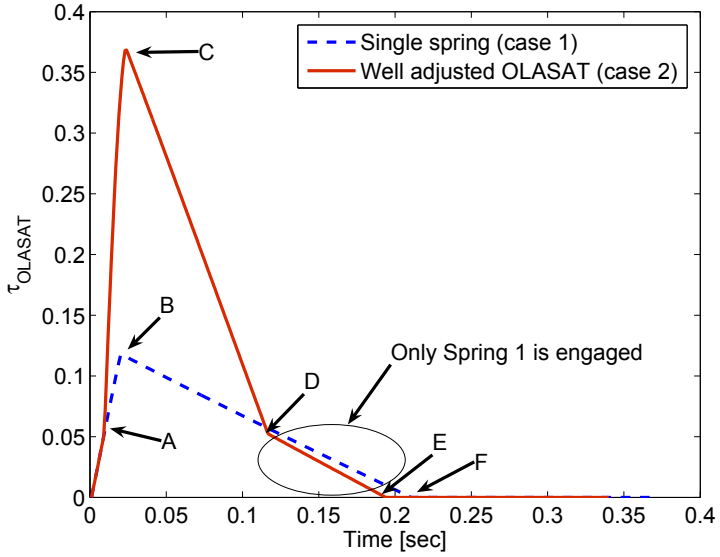

Fig. 16. Dimensionless torque of OLASAT vs. time during single support stance phase for both cases of single spring and OLASAT with well-adjusted stiffness.

that adaptive adjusting of K_{adjust}, as a function of the angular velocity of the stance leg at midstance, provides a better performance of the controller. Thus, in the simulation results of this section, the relation $K_{adjust} = 3l_2^{MD}\dot{\theta}_2$ is assumed. The controller is activated after the first walking step by sensing the angular velocity of the stance leg at midstance. As shown in Fig. 17, the sudden change in the velocity of the COM of the body is significantly reduced with compare to both the single spring and fixed stiffness. The energy loss is also significantly reduced, $\Delta\kappa = 0.052$, compared to case 1 and 2.

7. Conclusions

This work introduced different designs of adjustable stiffness artificial tendons. The modeling and detail conceptual design of each tendon were given. Then the results of the effects of stiffness adjustment of the ankle joint on energetics of the bipedal walking robots were presented. A methodology to reduce the energy loss was presented through three main efforts. In the first effort, one of the adjustable-stiffness artificial tendon, named OLASAT, was selected which is capable of storing and releasing the elastic energy during walking. In the second effort, a simplified model of the bipedal walking robot in the stance phase was developed which consists of a foot, a leg and an OLASAT which is installed parallel to the ankle joint. Such a model was used to compare the effects of a single spring and a well-adjusted stiffness OLASAT on reducing the energy loss during foot-touch-down. As the third effort, a simple controller based on energy feedback was designed to adjust the stiffness of OLASAT. Computer simulations were carried out to compare the energy loss of the biped in the two cases of the single spring and the well-adjusted stiffness OLASAT.

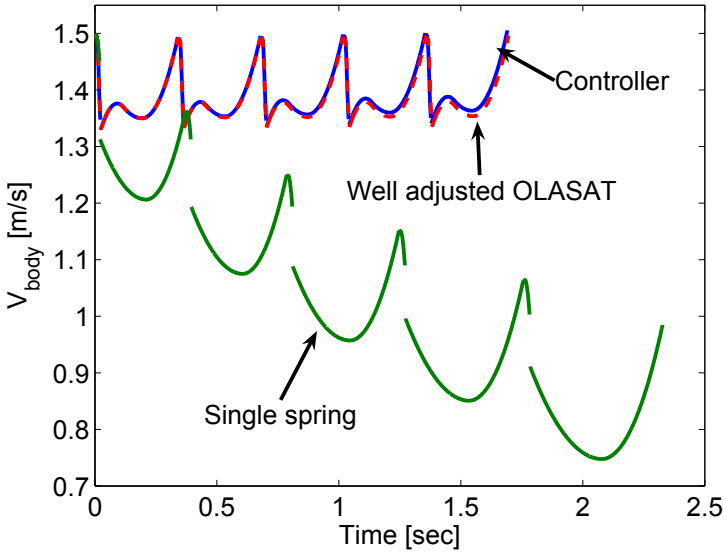

Fig. 17. Velocity of COM of the body vs time during 5 multiple walking steps for three cases of single spring, OLASAT with well-adjusted stiffness and stiffness adjustment controller.

Proper adjustment of the stiffness significantly reduces the kinetic energy loss during the foot-touch-down from 20% (of the single spring) to 1%. Simulation results of the biped during multiple walking steps illustrate that proper stiffness adjustment of OLASAT significantly improves the energetics of the bipedal walking. On average, the kinetic energy loss during multiple walking steps is reduced from 8% to 0.5% in each walking step. Simulation results illustrated that the automated stiffness adjustment controller can successfully reduce the energy loss during the stance phase. In general, the simulation results of this work suggest that various designs of the adjustable stiffness artificial tendons can be included in robot structures to achieve better energetics.

8. References

Alexander, R. M. (1988). *Elastic mechanisms in animal movement*, Cambridge University Press.

Alexander, R. M. & Bennett, M. B. (1989). How elastic is a running shoe?, *New Scientist* **123**: 45–6.

Bicchi, A. & Tonietti, G. (2004). Fast and soft-arm tactics [robot arm design], *IEEE Robotics and Automation Magazine* **11(2)**: 22–33.

Cavagna, G. A., Heglund, N. G. & Taylor, C. R. (1977). Mechanical work in terrestrial locomotion: two basic mechanisms for minimizing energy expenditure, *American Journal of Physiology* **233**: 243–261.

Cavagna, G. A., Saibene, F. P. & Margaria, R. (1964). Mechanical work in running, *Journal of Applied Physiology* **19**: 249–256.

Coleman, M. & Ruina, A. (1998). An uncontrolled toy that can walk but cannot stand still, *Physical Review Letters* **80(16)**: 3658–3661.

Collins, S. H., Wisse, M. & Ruina, A. (2001). A three-dimensional passive-dynamic walking robot with two legs and knees, *International Journal of Robotics Research* **20(7)**: 607–615.

Donelan, J.M. Kram, R. & Kuo, A. (2002). Mechanical work for step-to step transitions is a major determinant of the metabolic cost of human walking, *Journal of Experimental Biology* **205**: 3717–3727.

Donelan, M. J., Kram, R. & Kuo, A. D. (2002). Simultaneous positive and negative external mechanical work in human walking, *Journal of Biomechanical Engineering* **35**: 117–124.

Farley, C. T., Glasheen, J. & McMahon, T. A. (1993). Running springs: speed and animal size, *Journal of Experimental Biology* **185**: 71–86.

Farley, C. T. & Gonzalez, O. (1996). Leg stiffness and stride frequency in human running, *Journal of Biomechanics* **29**: 181–186.

Ferris, D. P., Louie, M. & Farley, C. T. (1998). Running in the real world: adjusting leg stiffness for different surfaces, *The Royal Society B: Biological Sciences* pp. 989–994.

Garcia, M. S. (1999). *Stability, scaling, and chaos in passive dynamic gait models*, PhD thesis, Theoretical and Applied Mechanics, Cornell University.

Geyer, H. (2005). *Simple models of legged locomotion based on compliant limb behavior*, PhD thesis, University of Jena.

Geyer, H., Blickan, R. & Seyfarth, A. (2002). Natural dynamics of spring–like running–emergence of self stability, *5th International Conference on Climbing and Walking Robots* pp. 87–91.

Geyer, H., Seyfarth, A. & Blickhan, R. (2005). Spring–mass running: simple approximate solution and application to gait stability, *Journal of Theoretical Biology* **232(3)**: 315–328.

Ghorbani, R. (2008). *On controllable stiffness bipedal walking*, PhD thesis, Mechanical and Manufacturing Engineering, University of Manitoba.

Ghorbani, R. & Wu, Q. (2009a). Conceptual design of the adjustable stiffness artificial tendons for legged robotics, *Mechanism and Machine Theory* **44(1)**: 140–161.

Ghorbani, R. & Wu, Q. (2009b). On improving bipedal walking energetics through adjusting the stiffness of elastic elements at the ankle joint, *International Journal of Humanoid Robots, In revision* **6(1)**: 23–48.

He, J. P., Kram, R. & McMahon, T. A. (1991). Mechanics of running under simulated low gravity, *Journal of Applied Physiology* **71**: 863–870.

Howard, R. D. (1990). *Joint and actuator design for enhanced stability in robotic force control*, PhD thesis, Massachusetts Institute of Technology.

Hurst, J., Chestnutt, J. & Rizzi, A. (2004). An actuator with physically variable stiffness for highly dynamic legged locomotion, *International Conference on Robotics and Automation* pp. 4662–4667.

Hurst, J. & Rizzi, A. (2004). Physically variable compliance in running, *International Conference on Climbing and Walking Robots* pp. 123–132.

Kuo, A. D., Donelan, J. M. & Ruina, A. (2005). Energetic consequences of walking like an inverted pendulum: step-to-step transitions, *Exercise and Sport Sciences Reviews* **33(2)**: 88–97.

McGeer, T. (1990). Passive dynamic walking, *The International Journal of Robotics Research* **9**: 62–82.

McMahon, T. & Cheng, G. (1990). The mechanics of running: how does stiffness couple with speed, *Journal of Biomechanics* **23 (Suppl. 1)**: 65–78.

Norton, R. L. (1999). *Design of machinery*, Thomas Casson.

Pratt, G. A. & Williamson, M. (1995). Series elastic actuators, *IEEE International Conference on Intelligent Robots and Systems* pp. 399–406.

Roberts, T. J., Marsh, R. L., Weyand, P. G. & Taylor, C. R. (1997). Muscular force in running turkeys: the economy of minimizing work, *Science* **275**: 1113–1115.

Robinson, D. W., Pratt, J. E., Paluska, D. J. & Pratt, G. A. (1999). Series elastic actuator development for a biomimetic walking robot, *Advanced Intelligent Mechatronics* pp. 19–22.

Seyfarth, A. (2000). *Elastically Operating Legs – Strategies and Construction Principles*, PhD thesis, University of Jena.

Vanderborght, B., Verrelst, B., Van Ham, R., Van Damme, M., Lefeber, D., Duran, B. M. Y. & Beyl, P. (2006). Exploiting natural dynamics to reduce energy consumption by controlling the compliance of soft actuators, *The international Journal of Robotics Research* **25(4)**: 343–358.

Veneman, J., Ekkelenkamp, R., Kruidhof, R. & van der Helm, F. C. T. (2006). A series elastic– and bowden–cable–based actuation system for use as torque actuator in exoskeleton-type robots, *The international Journal of Robotics Research* **25(3)**: 261–281.

Williamson, M. M. (1995). *Series elastic actuators*, PhD thesis, Massachusetts Institute of Technology.

Wisse, M. (2004). *Essentials of dynamic walking: analysis and Design of Two-Legged Robots*, PhD thesis, T.U. Delft.

Wisse, M. & Frankenhuyzen, J. V. (2006). Design and construction of mike; a 2d autonomous biped based on passive dynamic walking, *Adaptive Motion of Animals and Machines* pp. 143–154.

Zinn, M., Roth, B., Khatib, O. & Salisbury, J. K. (2004). New actuation approach for human friendly robot design, *The International Journal of Robotics Research* **23(4-5)**: 379–398.

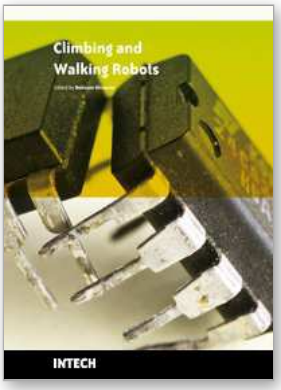

Climbing and Walking Robots

Edited by Behnam Miripour

ISBN 978-953-307-030-8
Hard cover, 508 pages
Publisher InTech
Published online 01, March, 2010
Published in print edition March, 2010

Nowadays robotics is one of the most dynamic fields of scientific researches. The shift of robotics researches from manufacturing to services applications is clear. During the last decades interest in studying climbing and walking robots has been increased. This increasing interest has been in many areas that most important ones of them are: mechanics, electronics, medical engineering, cybernetics, controls, and computers. Today's climbing and walking robots are a combination of manipulative, perceptive, communicative, and cognitive abilities and they are capable of performing many tasks in industrial and non- industrial environments. Surveillance, planetary exploration, emergence rescue operations, reconnaissance, petrochemical applications, construction, entertainment, personal services, intervention in severe environments, transportation, medical and etc are some applications from a very diverse application fields of climbing and walking robots. By great progress in this area of robotics it is anticipated that next generation climbing and walking robots will enhance lives and will change the way the human works, thinks and makes decisions. This book presents the state of the art achievments, recent developments, applications and future challenges of climbing and walking robots. These are presented in 24 chapters by authors throughtot the world The book serves as a reference especially for the researchers who are interested in mobile robots. It also is useful for industrial engineers and graduate students in advanced study.

How to reference

In order to correctly reference this scholarly work, feel free to copy and paste the following:

Reza Ghorbani and Qiong Wu (2010). On Adjustable Stiffness Artificial Tendonsin Bipedal Walking Energetics, Climbing and Walking Robots, Behnam Miripour (Ed.), ISBN: 978-953-307-030-8, InTech, Available from: http://www.intechopen.com/books/climbing-and-walking-robots/on-adjustable-stiffness-artificial-tendonsin-bipedal-walking-energetics

INTECH
open science | open minds

InTech Europe
University Campus STeP Ri
Slavka Krautzeka 83/A
51000 Rijeka, Croatia
Phone: +385 (51) 770 447
Fax: +385 (51) 686 166

InTech China
Unit 405, Office Block, Hotel Equatorial Shanghai
No.65, Yan An Road (West), Shanghai, 200040, China
中国上海市延安西路65号上海国际贵都大饭店办公楼405单元
Phone: +86-21-62489820
Fax: +86-21-62489821